

Polymorphism of two-dimensional antiferromagnets, AgF_2 and CuF_2

Daniel Jeziarski* and Wojciech Grochala*

*d.jeziarski@cent.uw.edu.pl, w.grochala@cent.uw.edu.pl

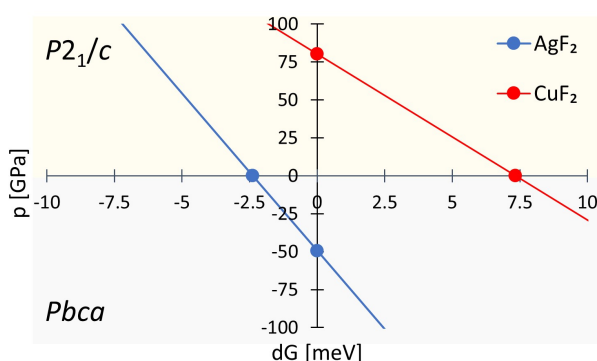
Center of New Technologies, University of Warsaw, 02089 Warsaw Poland

This work is dedicated to Professor Jacek Klinowski at his 80th birthday

Abstract

We present theoretical study of relative stability as well as of the magnetic and electronic properties of AgF_2 and CuF_2 , in two related structural forms: orthorhombic (ambient pressure form of AgF_2) and monoclinic (ambient pressure form of CuF_2), using Density Functional Theory. We show, that at $P2_1/c \rightarrow Pbc_a$ structural transition is associated with weakening of intra-sheet magnetic superexchange. This finding is consistent with the flattening of 2D layers, smaller charge-transfer energy and stronger admixing of $\text{Ag}_d/\text{Cu}_d\text{-F}_p$ states in monoclinic structure, comparing to orthorhombic form. Consequently, monoclinic AgF_2 should be targeted in experiment as it should show stronger magnetic coupling than its orthorhombic sibling. The dynamically stable $P2_1/c$ form of AgF_2 could be achieved via two alternative paths: by applied negative strain, or by rapid quenching silver(II) difluoride from temperatures higher than 480 K to low temperatures.

Graphical abstract



Keywords

layered materials, antiferromagnets, polymorphism, pressure, phase diagram

Introduction

The most typical structure adopted by transition metal difluorides at ambient pressure is rutile type (Fig. 1). For TMF_2 , where $\text{TM} = \text{V}, \text{Mn}, \text{Fe}, \text{Co}, \text{Ni}, \text{Pd}, \text{Zn}$, difluorides crystallize in tetragonal system $P4_2/mnm$ space group^[1-3]. Building blocks in this structure consist of nearly regular octahedra of fluorine atoms around each metal ion ($\text{CN}=6$), with both edge and corner sharing of F atoms. However, in the case of CrF_2 ^[4] and CuF_2 ^[5], the deformation of octahedra is pronounced, predominantly due to the Jahn-Teller effect. Here, the elongation of apical M-F bonds leads to the symmetry lowering, with the resulting monoclinic structure ($P2_1/c$). Another important structural type among metal difluorides is fluorite with a cubic ligand environment around metal cation ($\text{CN}=8$). However, among TM systems, this type is adopted only by three difluorides: two with closed-shell cations - CdF_2 , HgF_2 (which could be classified as post-transition ones) and only one with a genuine open d-shell cation – AgF_2 . For the latter, Jahn-Teller effect drives the distortion from the parent cubic polytype towards the orthorhombic one (Pbc_a)^[6]. Thus, both CuF_2 and AgF_2 exemplify the unique low-symmetry structures types, otherwise unknown among ionic fluorides.

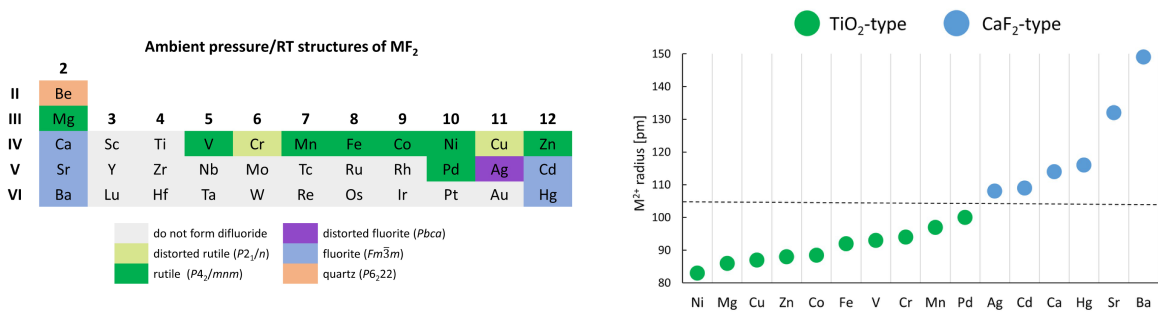


Fig. 1 Ambient pressure/room temperature structure of selected MF₂ (left) and type of structure adopted of binary difluorides depending on the M²⁺ ionic radius in octahedral environment (right). The dashed line indicates the boundary between two structure types: rutile and fluorite.

Polymorphism of metal difluorides is even richer at elevated pressure conditions, as extensively studied during the last years^[3,7-14]. Most TM difluorides adopt close-packed cotunnite (*Pnma*) structure (CN=9) upon compression, with Ni₂In-type (CN=11) as an ultimate high-pressure structure. For example, FeF₂ undergoes the following sequence of phase transitions: rutile → CaCl₂ → Ni₂In, thus the CN of metal atom increasing from 6 via 9 to 11. Another example is NiF₂, where compression up to 3 GPa induces rutile → CaCl₂ transformation^[10]. However, theoretical study predicts that at 30 GPa this compound should adopt monoclinic structure (*C2/c*), and this remains to be verified in experiment^[15]. Additionally, there are two examples of difluorides where cotunnite structure has not yet been observed experimentally. The first example is PdF₂ (with high-spin d⁸ cations) where rutile → cubic (*Pa $\bar{3}$*) transformation occurs at 1.5 GPa^[3]; the cubic polytype can be also stabilized in the low-temperature regime^[16]. The second one is AgF₂ which undergoes the following transitions: *Pbca* → *Pca2₁* → *Pbcn* → *Pnma*^[13], with two unusual intermediate forms: a non-centrosymmetric *Pca2₁* one and a unique nanotube-like *Pbcn*. A similar sequence is theoretically predicted for its lighter congener, CuF₂^[11]. Indeed, the *P2₁/c* → *Pbca* (AgF₂-type) transition was observed for CuF₂ at 9 GPa, while the PbCl₂-type structure is predicted theoretically to occur only at 72 GPa^[11]. Clearly, CuF₂ and AgF₂ behave quite differently from the rest of the TM difluoride herd.

Polymorphism strongly affects key material properties such as e.g. magnetic and electronic ones. We note that both AgF₂ and CuF₂ are layered, with corrugated sheets constructed from [MF₄] units (Fig.2). Still, the disparate stacking of sheets and quite different nature of M-F bonds in both compounds (more covalent for Ag, more ionic for Cu), strongly affect their physicochemical properties. Silver difluoride in many ways mimics undoped oxocuprates (HTSC precursors)^[17-19], and diverse ways of its doping have been theoretically^[20-24] and experimentally^[25] explored. As a result of these efforts, we have recently observed the coexistence of two structural types of solid solutions in Cu-Ag-F phase diagram: monoclinic (CuF₂-type) and orthorhombic (parent AgF₂-type) (Fig.2)^[25]. Their formation is unexpected due to substantial difference in the cation size ($R_{Cu^{2+}} = 0.87 \text{ \AA}$ and $R_{Ag^{2+}} = 1.08 \text{ \AA}$) across the rutile/fluorite boundary (Fig.1). Interestingly, despite that, at experiment conditions discussed in Ref.25, as much as 44% of Ag could be doped into CuF₂ structure, and up to 30 % Cu into the AgF₂ type. The formation of mixed-cation phases raises a natural question: could Cu-free AgF₂ be obtained in the monoclinic form, or Ag-free CuF₂ in the orthorhombic form, and what would be the key properties of these polymorphs? The experimental results suggest that CuF₂ may indeed be pushed into AgF₂ type at elevated pressure^[9] but it is not known yet whether the high-pressure type is quenchable to ambient (p,T) conditions, and what its properties would be. On the other hand, whether AgF₂ could be obtained in the CuF₂ type is an open question.

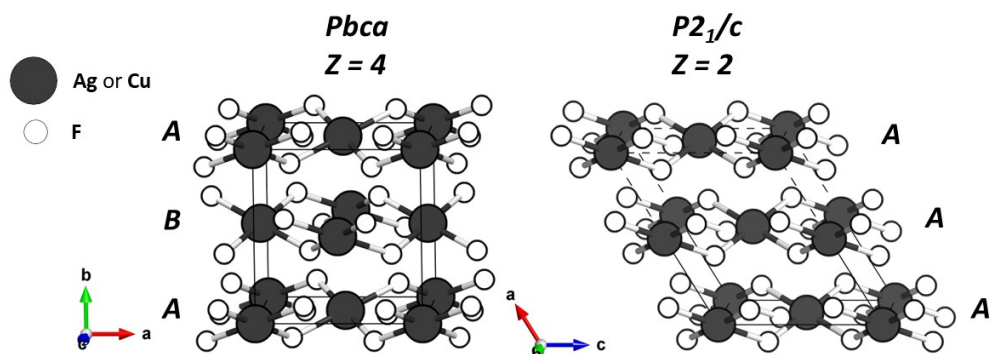


Fig. 2 The ambient pressure structures of AgF_2 $Pbca$ (left) and CuF_2 $P2_1/c$ (right). Only intra-layer M-F bonds are shown for clarity. *ABA* and *AAA* marks refer to the type of layer stacking. In case of $P2_1/c$ structure, $1 \times 2 \times 1$ supercell is presented for direct comparison with the orthorhombic structure.

Motivated by these findings, in this paper we theoretically study the dynamic and thermodynamic stability of four phases i.e. CuF_2 and AgF_2 each in two different structure types, and we evaluate their key electronic and magnetic properties. Finally, we propose possible experimental pathway to obtain the Cu-free monoclinic AgF_2 .

Methods

Calculations were performed within the DFT approach as implemented in VASP 5.4.4 code^[26], using a GGA-type PBEsol^[27] functional with projected augmented wave method^[28,29]. The on-site Coulombic interactions of d electrons were realized by introducing Hubbard (U_d) and Hund (J_H) parameters (DFT+U formalism), as proposed by Liechtenstein^[30]. In DFT+U and DFT+U+vdW methods, the J_H was set to 1 eV^[31], while the U_d value was set to 8 and 10 eV, respectively for Ag and Cu^[32,33], where van der Waals dispersion energy-correction term was provided following the expression introduced by Grimme et al. (DFT-D3)^[34]. Two other methods have been also employed: SCAN and HSE06. Plane-wave cutoff energy of 520 eV was used in all systems. The k-spacing was set to 0.032 \AA^{-1} for geometry optimization and 0.022 \AA^{-1} for self-consistent-field convergence. The convergence thresholds of 10^{-7} eV for electronic and 10^{-5} ionic steps were used. Calculations of phonon curves for each structure were realized using PHONOPY package^[35] (step-by-step procedure is available online, on the official website). ZPE energies/ Γ -point frequencies, were calculated using DFPT or finite differences approaches provided by VASP software.

Results and discussion

1.1. Structural features of silver and copper difluorides in both polymorphic forms

For AgF_2 in its $Pbca$ type, the first coordination sphere of cation, can be described as deformed rhombic prism (2+2+2+2 coordination), while for CuF_2 in its parent $P2_1/c$ structure, as an elongated octahedron (4+2 coordination) (**Fig.3**).

Our theoretical calculations nicely reproduce experimental structural parameters of AgF_2 and CuF_2 in their most stable structures (**Table 1**). The best agreement between experimental and theoretical volumes of the unit cell was found using SCAN method. The fully optimized AgF_2 and CuF_2 unit cells differs in volume only by 1.75% and 1.66%, respectively, to experimental ambient pressure and ambient temperature forms^[6,36]. Comparable results come from HSE06 method, where volume differ by 1.67% and 1.96%, respectively, for silver and copper difluoride from experimental data. The DFT+U method with van der Waals correction, gives worse agreement – volumes of optimized unit cells are underestimated by 5.51% and 7.02% compared to experimental ones, for AgF_2 and CuF_2 , respectively. However, since all calculations refer to $T \rightarrow 0 \text{ K}$ and $p \rightarrow \text{atm}$ 0 conditions, the discrepancies are expected; some are also related to the limitations of these theoretical methods. We note that adjustment of the U and J values, used in the spin polarized DFT calculations, may lead to better compatibility between experimental and theoretical structural parameters (see Tokar et. al^[37]

and Kurzydłowski^[11], where in DFT+U calculations $U = 5$ and $J = 1$ for AgF_2 and $U = 7$ and $J = 0.9$ eV for CuF_2 , respectively, give satisfactory agreement between experimental and theoretical structural parameters).

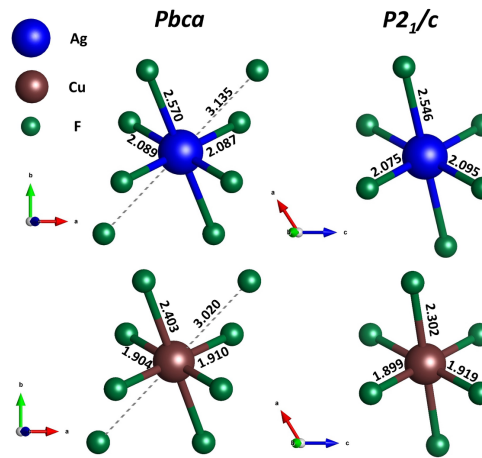


Fig. 3 First coordination sphere for AgF_2 (up) and CuF_2 (down) in $Pbca$ (left) and $P2_1/c$ (right) cells. The M-F bonds lengths are expressed in Å, following SCAN calculations.

Table 1. Unit cell parameters a , b , c , volumes V as estimated from experimental measurements (X-ray and neutron powder diffraction, XRPD and NPD) with theoretical values from our calculations for orthorhombic AgF_2 and monoclinic CuF_2 (for antiferromagnetic spin ground state). For orthorhombic cell all unit cell angles are equal 90° , where for monoclinic one $\alpha = \gamma = 90^\circ \neq \beta$.

Method	AgF_2 ($Pbca$)				Method	CuF_2 ($P2_1/c$)				
	a [Å]	b [Å]	c [Å]	V/FU [Å ³]		a [Å]	b [Å]	c [Å]	β [°]	V/FU [Å ³]
<i>PXRD</i> , RT ^[25]	5.550	5.836	5.095	41.257	<i>PXRD</i> , RT ^[25]	3.294	4.559	5.345	121.11	34.704
<i>NPD</i> , $4.2K$ ^[6]	5.524	5.780	5.066	40.438	<i>NPD</i> , $4.2K$ ^[36]	3.294	4.568	5.358	121.17	34.491
<i>XRD</i> , RT ^[26]	5.568	5.831	5.101	41.403	<i>PXRD</i> , RT ^[11]	3.302	4.560	5.352	121.11	34.497
<i>DFT+U</i>	5.433	5.768	5.008	39.234	<i>DFT+U</i>	3.192	4.505	5.293	121.32	32.510
<i>DFT+U+vdW</i>	5.408	5.660	4.993	38.211	<i>DFT+U+vdW</i>	3.185	4.479	5.286	121.72	32.068
SCAN	5.583	5.724	5.151	41.145	SCAN	3.302	4.522	5.310	121.20	33.917
HSE06	5.539	5.843	5.082	41.115	HSE06	3.296	4.516	5.300	120.98	33.817

Now, we will discuss the key structural differences between $Pbca$ and $P2_1/c$ structure type. There are three main structural differences between these structures: **1**) different stacking of $[\text{MF}_4]$ plaquettes i.e. ABA vs. AAA (**Fig. 1**); **2**) reduction of coordination number for M^{2+} from 8 to 6, and **3**) accompanying changes in the bond lengths and bond angles. Based on SCAN calculations, four intralayer (equatorial) Ag-F bond lengths in AgF_2 have similar values: 2×2.087 Å and 2×2.089 Å. The apical (axial) bonds are considerably longer: 2×2.570 Å. The last Ag-F contacts, completing the Ag^{2+} first coordination sphere, are significantly longer than the others: 2×3.135 Å. Similarly, for CuF_2 in $Pbca$ structure the first coordination sphere of cation includes the shortest contacts of 2×1.904 Å and 2×1.910 Å, the apical ones of 2×2.403 Å, and secondary interactions at 2×3.020 Å.

In the $P2_1/c$ system, the coordination sphere of M^{2+} is 6-fold (CN=6, **Fig. 2**). In AgF_2 , two intralayer Ag-F contacts are slightly shorter and two slightly longer than in the $Pbca$ structure: 2×2.075 Å and 2×2.095 Å. Apical bond lengths differ to a larger extent (2×2.546 Å in $P2_1/c$ form vs. 2×2.570 Å + 2×3.135 Å) i.e. they are shorter in monoclinic form (which is consistent with the reduction of the CN of the cation). In CuF_2 case, the intra-layer copper-fluoride bonds for the $P2_1/c$ form are 1.899 Å and 1.919 Å; however, the apical contacts are substantially shorter for this form (2×2.302 Å vs. 2×2.403 Å

+ 2x3.020 Å); this is consistent with the results previously reported by Kurzydłowski^[11]. Results from all computational methods indicate similar tendencies of bond length changes despite slight differences in absolute values (Table ESI 1-2).

Puckering of the MF₂ layers is also different in both structure types. For example, for the monoclinic AgF₂, the intra-layer Ag-F-Ag angle is larger by ca. 1.2° than in orthorhombic one (SCAN). For CuF₂ the effect is even more pronounced (3.0°). This may be related to the different metal-metal distances in both structures. In the P₂₁/c system Ag-Ag intra-layer distance is larger by 0.3%, whereas inter-layer contact is shorter by 2.8% compared to AgF₂ P_{bca} form. For copper difluoride, the intralayer Cu-Cu distances is by 1.3% larger, where interlayer one is by 8.0% shorter for P₂₁/c form (all values are listed in Table. S11-2 in ESI). All these features impact, as we will see, the magnetic and electronic properties of both polymorphs.

1.2. Dynamic stability

To evaluate dynamic stability, we calculated phonon modes at Gamma point for AgF₂ and CuF₂ in both polymorphic forms: P_{bca} and P₂₁/c (Table x ESI). Experimental (IR, RAMAN) and theoretical phonon frequencies of AgF₂ (P_{bca}) with their symmetry and optical activity, have been previously reported by Gawraczyński, et al^[17]. Additionally, Kurzydłowski^[11] previously assigned bands RAMAN active bands of CuF₂ (P₂₁/c). Here, we extended this assignment to IR-active CuF₂ bands of the monoclinic form. Additionally, we calculated dispersion of phonons for binary difluorides at P₂₁/c and P_{bca} structures in DFT+U framework (Fig. 4).

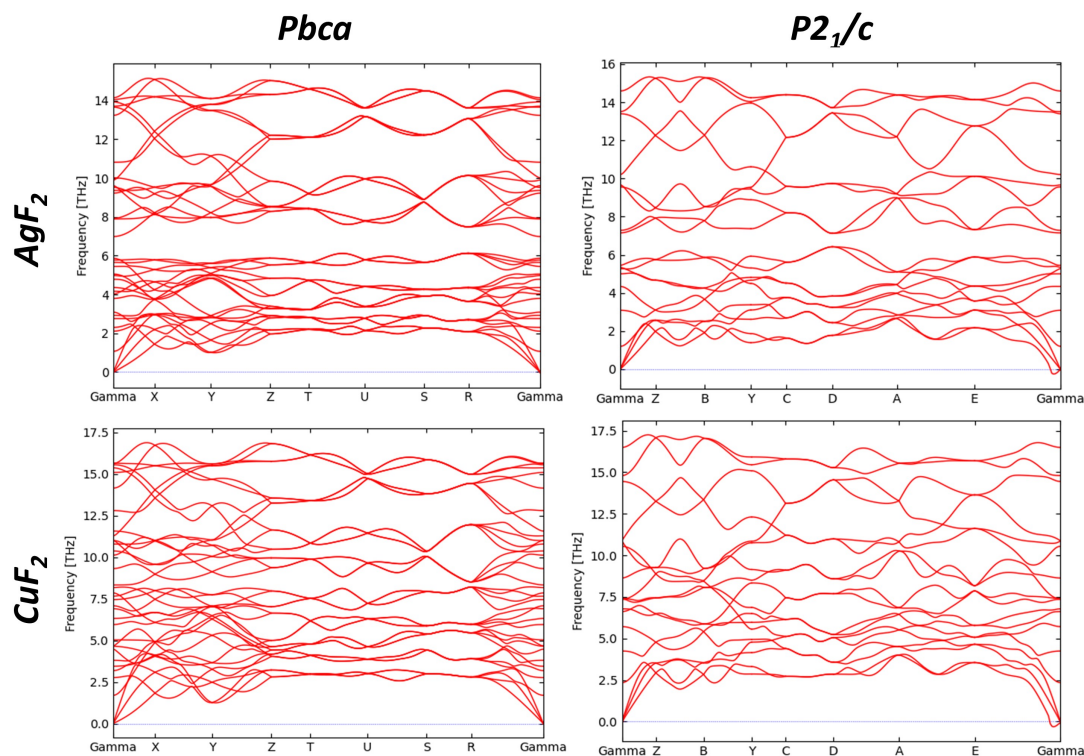


Figure 4. Phonon dispersion curves for AgF₂ (upper) and CuF₂ (lower) in P_{bca} (left) and P₂₁/c systems (right).

Analysis of phonon dispersion curves (Fig. 4) shows no dynamic instability for both compounds in orthorhombic system (P_{bca}). However, in monoclinic form (P₂₁/c), both compounds show very small soft features at q = (-0.04, 0.04, -0.04). This obviously is not an exact in reciprocal space, and indeed, geometry optimization of the structures obtained following the said imaginary mode do not lead to lower-energy (see SI4). In other words, tiny imaginary features off the zone center are purely

artificial. Lack of genuine imaginary modes suggests that monoclinic AgF₂ and orthorhombic CuF₂ are local minima at the potential energy surface and they could in principle be observed at T→0 K and p→0 GPa.

Table. 3 The list of Γ -point frequencies of the AgF₂ and CuF₂ compounds in *Pbca* and *P2₁/c* structures (DFT+U+vdW). Activity of modes in parentheses. Shadowed columns correspond to the translational modes. Frequency in cm⁻¹.

<i>Pbca</i>				<i>P2₁/c</i>			
#	AgF ₂ [cm ⁻¹]	CuF ₂ [cm ⁻¹]	Symm. (activity)	#	AgF ₂ [cm ⁻¹]	CuF ₂ [cm ⁻¹]	Symm. (activity)
1	478	526	B _{1g} (RAMAN)	1	493	560	B _g (RAMAN)
2	475	524	B _{2g} (RAMAN)	2	453	490	B _u (IR)
3	473	528	A _u (silent)	3	452	500	A _u (IR)
4	467	511	B _{1u} (IR)	4	355	389	A _g (RAMAN)
5	464	518	B _{3u} (IR)	5	333	373	A _u (IR)
6	450	476	B _{2u} (IR)	6	326	357	B _u (IR)
7	369	432	B _{2u} (IR)	7	241	294	B _g (RAMAN)
8	347	395	A _u (silent)	8	240	263	A _g (RAMAN)
9	332	388	B _{3g} (RAMAN)	9	183	250	B _u (IR)
10	329	372	B _{1u} (IR)	10	180	254	A _u (IR)
11	325	371	B _{3u} (IR)	11	175	235	B _g (RAMAN)
12	324	369	B _{3g} (RAMAN)	12	158	220	A _u (IR)
13	307	347	A _g (RAMAN)	13	149	192	B _u (IR)
14	274	318	B _{1g} (RAMAN)	14	108	145	A _u (IR)
15	273	357	B _{2g} (RAMAN)	15	54	75	A _g (RAMAN)
16	240	242	A _g (RAMAN)	16	0	0	B _u
17	203	267	B _{3u} (IR)	17	0	2	A _u
18	197	261	B _{1u} (IR)	18	1	1	B _u
19	191	254	A _u (silent)				
20	186	283	B _{1g} (RAMAN)				
21	172	231	A _u (silent)				
22	172	236	B _{2u} (IR)				
23	165	203	B _{2u} (IR)				
24	148	172	B _{3u} (IR)				
25	148	160	B _{1u} (IR)				
26	137	157	B _{2g} (RAMAN)				
27	136	231	B _{3g} (RAMAN)				
28	114	160	A _u (silent)				
29	105	126	B _{2u} (IR)				
30	99	113	B _{3u} (IR)				
31	90	104	A _u (silent)				
32	79	180	A _g (RAMAN)				
33	45	71	B _{1u} (IR)				
34	0	1	B _{2u}				
35	1	2	B _{1u}				
36	1	1	B _{3u}				

On the basis of Group Theory, for the $P2_1/c$ structure ($Z=2$), among the 18 Γ -point optical modes 9 are IR-active ($5A_u + 4B_u$) and 6 are Raman-active ($3A_g + 3B_g$). For $Pbca$ structure Group Theory predicts that 15 modes are IR-active ($5B_{1u} + 5B_{2u} + 5B_{3u}$), 12 are Raman-active ($3A_g + 3B_{1g} + 3B_{2g} + 3B_{3g}$) and 6 are silent (A_u). The theoretical results obtained from all theoretical methods used in this work are presented in *Supplementary Information* (Table SI8-SI11, ESI). Here we show theoretical frequencies of the modes, their symmetry and activity, following DFT+U+vdw results only (**Table 3**).

The good agreement between theoretical and experimental values of the mode frequencies reflects the precision of the DFT method (Table SI7, ESI). Moreover, translations (acoustic modes) are computed with $\pm 2 \text{ cm}^{-1}$ error bar, suggesting that optical frequencies may have a similarly small error.

Raman and IR spectroscopies are very powerful tools in the detection of structural transitions of compounds as they give insight into the local environment of atoms and can be easily equipped with e.g. diamond anvil cell (DAC) used in high-pressure studies. Therefore, analysis of RAMAN and IR spectra may be suitable for disclosure of possible structural transition of AgF_2 . To anticipate changes on the spectra during such a transition, we will now analyze IR- and RAMAN-active modes for AgF_2 and, also, for CuF_2 in both structural forms. We note that the evolution of RAMAN spectra of CuF_2 upon pressure, has recently been employed to detect $P2_1/c \rightarrow Pbca$ transition^[11]. Thus, this work complets previous research by including data of IR-active modes for this compound, in its both structural forms.

Based on **Table 3**, there are clear differences in the fundamental phonons, between AgF_2 and CuF_2 , in two polymorphic forms. The symmetry-related modes (e.g. B_{1g} in both compounds in orthorhombic form) have higher frequencies in case of copper difluoride. In the simplest harmonic approximation, the vibration energy is proportional to the bonding strength (force constant) and inversely proportional to the mass of interacting atoms (reduced mass). Although, the M-F bond is more covalent in AgF_2 than in CuF_2 ^[18,39,40], the reduced mass seems to be a dominant factor of the aforementioned changes in the frequencies of modes; mass of Cu constitutes only ca. 60% of atomic mass of Ag.

Regarding the experimentally-related issue, transition from monoclinic to orthorhombic structure of AgF_2 should be accompanied with reduction of the number of band appearing in both IR and RAMAN spectra, from 27 to 15 optically active modes. Additionally, $Pbca \rightarrow P2_1/c$ transition should be reflected in the changes of the frequencies of symmetry-related modes. For instance, the sudden change of $15\text{-}18 \text{ cm}^{-1}$ is expected, between symmetry-related B_{1g} (478 cm^{-1}) and B_{1g} (475 cm^{-1}) modes for $Pbca$ and B_g (493 cm^{-1}) for $P2_1/c$ polymorphs. This trend of mode stiffening is more general, as the ZPE value is predicted to be higher by 7 meV/FU (**Table 4**) for $P2_1/c$ form, than that, for the ambient pressure form of silver difluoride. This emerges partially from the changes in the average value of associated bond lengths. Based on the theoretical results, the shortening by approx. 0.1% and 0.9%, for equatorial and axial M-F bonds, respectively, following $Pbca \rightarrow P2_1/c$ transformation, should indeed take place for AgF_2 . Same trend holds for CuF_2 .

1.3. Energetic and thermodynamic stability of both polymorphs

Comparing ground state energies of binary fluorides in $P2_1/c$ and $Pbca$ systems (including zero-point energies) and volume changes (dV) arising from their structure modification, we may estimate the relative stability of both polymorphs as well as transition pressure of $P2_1/c \rightarrow Pbca$ transformation for both compounds. In doing so we follow equation $p = \frac{dE}{dV}$ (1) and assume so called common tangent approximation. The results obtained with the state of the art DFT+U+vdW method are listed in **Table 4** (for all methods tested cf. Table SI3-SI4 in ESI).

Copper difluoride in the $Pbca$ structure is uphill by 80 meV per FU (including ZPE) as compared to monoclinic form; this explains persistence of the latter in experiment at ambient (p, T) conditions. However, the volume of $Pnma$ form is by $1.65\text{-}1.76 \text{ \AA}^3$ smaller than in case of the monoclinic form,

suggesting that orthorhombic form could be achieved at elevated pressure. Our computed transition pressure of 7.3 GPa is only slightly underestimated (experimental value is 1.7 GPa larger^[11]).

Table 4. Ground state energies (E_{GS}), volumes of unit cell (V), zero-point energies (ZPE), transition pressure (p) including zero-point energy (p_{ZPE}), transition temperature from ambient pressure structure without (T) and with zero-point energy (T_{ZPE}). Data within DFT+U+vdW method. Results from all methods presented in *Supplementary Information*, Table. SI4-SI5

AgF ₂	E_{GS}/FU [eV]	V/FU [Å ³]	ZPE [eV]	p [GPa]	p_{ZPE} [GPa]	T [K]	T_{ZPE} [K]
<i>P2₁/c</i>	-9.224	40.995	0.121	-2.8	-2.4	573	480
<i>Pbca</i>	-9.273	38.211	0.129				
CuF ₂	E_{GS}/FU [eV]	V/FU [Å ³]	ZPE [eV]	p [GPa]	p_{ZPE} [GPa]	T [K]	T_{ZPE} [K]
<i>P2₁/c</i>	-11.626	32.068	0.143	6.3	7.3	805	933
<i>Pbca</i>	-11.557	30.311	0.154				

In case of AgF₂, relative stability of two structures depends on the method used (see ESI). For DFT+U+vdW standard the *Pbca* form is more stable than monoclinic form by 49 meV (including ZPE). On the other hand, unit cell volume of AgF₂ in *Pbca* form is ca. 1.7 Å³ smaller than in *P2₁/c*. Therefore, according to the equation 1, calculated pressure of transition must be negative. Here, we obtain the value of ca. -2.4 GPa with DFT+U+vdW (**Table 4**). Since the ambient (p,T) form of AgF₂ is orthorhombic (*Pbca*), we believe that employment of van der Waals functional is necessary for a proper description of the relative stability. Nevertheless, the formally negative value of transition pressure, while unphysical, may to some extent be mimicked by negative strain (e.g. in epitaxial deposition techniques). On the other hand, one may estimate temperature needed for structural transition to take place. In case of silver difluoride, the estimated temperature for *Pbca* → *P2₁/c* structural transformation is equal ca. 450 K (with ZPE correction). We will return to this finding below.

1.4. Electronic and magnetic properties

The **Fig. 5** presents electronic density of states for copper and silver difluorides in two structures: *Pbca* and *P2₁/c*. The value of fundamental band gap, calculated for AgF₂ (*Pbca*) is consistent within three methods used: DFT+U+vdW and HSE06, and equals ca. 2.17-2.18 eV (**Table 4**). However, for SCAN method yields a severely underestimated value of BG of 0.52 eV. Since experimentally determined charge-transfer gap according to the ZSA scheme^[41] is ca. 3.4 eV^[19], we conclude that even HSE06 method underestimates the gap. For monoclinic form of AgF₂ (*P2₁/c*), calculated charge-transfer gap is approx. 1.94-1.96 eV (within DFT+U+vdW and HSE06). These values are 11 % smaller than the gap computed for orthorhombic form so, given error cancelling, we expect that experimentally determined BG for monoclinic form would indeed be smaller than that for orthorhombic form (89% of 3.4 eV yields ca. 3.0 eV).

The changes of the band gap value with structural transformation are also observed in case of CuF₂. For the ambient pressure form of copper difluoride, the DFT+U+vdw method gives BG of 4.46 eV, while HSE06 predicts a somewhat smaller value of 4.14 eV. To the best of our knowledge, there is no experimental estimate of the band gap value for CuF₂. However, our theoretical results are in line with previously reported calculations by Miller and Botana^[40]. It may be expected that the band gap for more ionic CuF₂ should indeed be larger than for more covalent AgF₂. Again, as for AgF₂, calculations predict larger gap for orthorhombic than for the monoclinic form (by 4% and 7%, following DFT+U+vdw and HSE06 results, respectively). To verify this result, high-pressure form of CuF₂ should first be quenched to ambient (p,T) conditions and its band gap examined.

The result obtained for AgF_2 agree qualitatively with the Maximum Hardness Principle (MHP) by Pearson^[42] as a broader gap ($Pbca$) form is more stable (at $p \rightarrow 0$ atm, $T \rightarrow 0$ K) than a narrower-gap $P2_1/c$ form. Interestingly, contradictory observation can be made for CuF_2 .

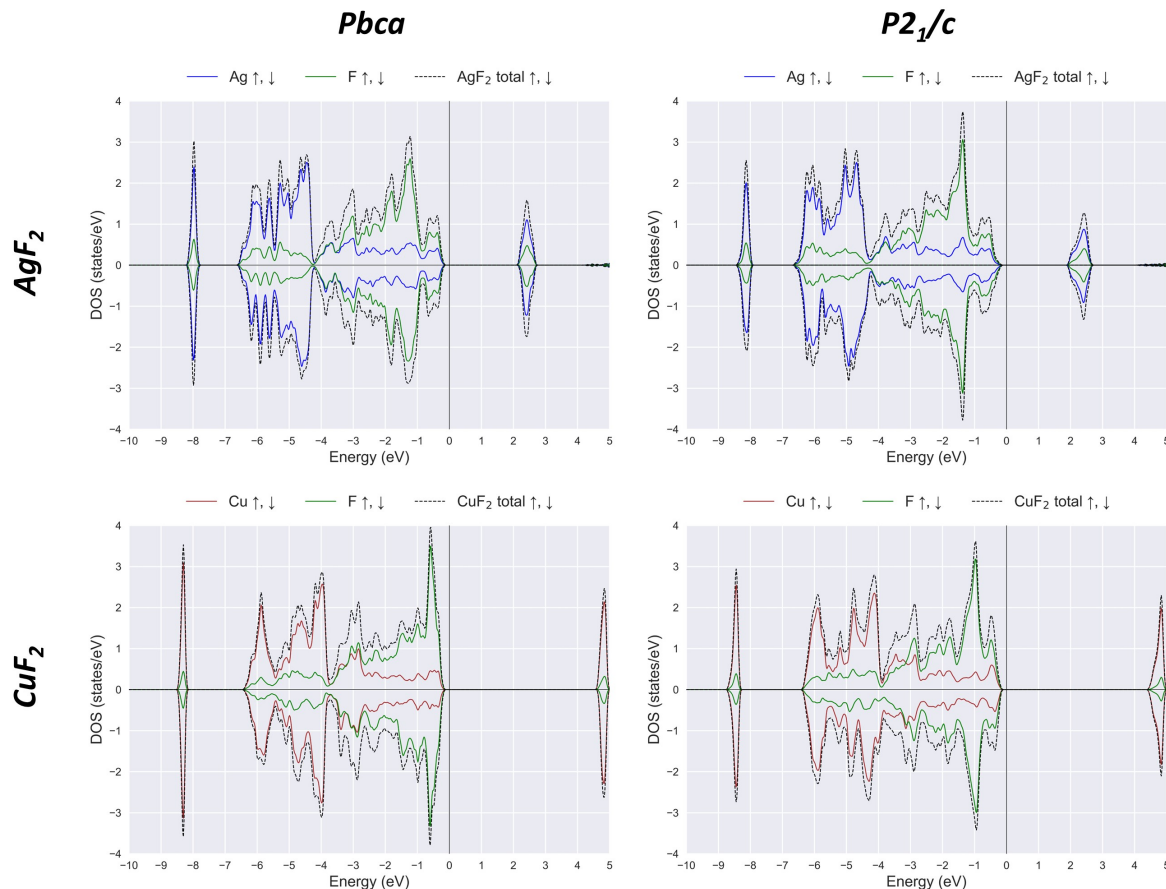


Fig. 5 Atom-resolved eDOS for AgF_2 (upper) and CuF_2 (lower) in $Pbca$ and $P2_1/c$ systems calculated within DFT+U+vdW method. For eDOS from HSE06 method, please check **Fig. S11** in ESI.

The inspection of density of states (DOS presented on **Fig. 5**) indicates, that between $P2_1/c$ and $Pbca$ forms of AgF_2 , there are some differences regarding contributions from silver and fluorine states to conduction and valence bands. In case of orthorhombic form of silver difluoride (ambient pressure), the major contribution to valence band (at the vicinity of Fermi level) comes from F_p states, whereas, the conduction band (i.e. upper Hubbard band, UHB) is mainly formed by Ag_d states. In case of monoclinic form, one may note a stronger admixture of Ag and F states in both bands. This indicates increased Ag-F bond covalence, in agreement to the changes of bond lengths and optical phonon frequencies. This tendency is even more evident in case of CuF_2 (**Fig. 5**, bottom part). Here, again, monoclinic form shows greater hybridization of Cu_d - F_p states than the orthorhombic one.

The width of Upper Hubbard Band (conduction band) is another important parameter related to possible electron doping to both compounds.^[22,43] Our results indicate, that in both compounds, the UHB is slightly widened in $P2_1/c$ structure as compared to $Pbca$ one. For this reason, AgF_2 in monoclinic structure might be more feasible to dope, than in its ambient (p,T) form^[21].

As AgF_2 and CuF_2 are two-dimensional antiferromagnets (for AgF_2 the $T_N = 163\text{K}$ ^[44], whereas for CuF_2 , $T_N = 69\text{K}$ ^[45]), the strength of magnetic superexchange, J_{2D} , is of interest. Experimentally determined J_{2D} value for AgF_2 is equal ca. -70 meV^[17] (negative sign indicates antiferromagnetic interaction). The SCAN predicts very similar value: -67.3 meV; in DFT+U method, the superexchange value is twice as low (**Table 5**). In case of CuF_2 , limited information is available on the experimentally determined value of the intra-sheet magnetic superexchange constant. To the best of our knowledge,

there is only one experimental paper, where authors claim the magnitude of J_{2D} to be -2.9 meV^[45], on the basis of magnetic measurements. However, sophisticated computational method predicts it to be *ca.* -11 meV^[46]. Our calculations are not so far from the latter; DFT+U+vdW predicts value of -8.2 meV. On the other hand, SCAN and HSE06 methods predict higher absolute value of J_{2D} i.e. -21.6 meV and -18.3 meV, respectively (**Table 5**). The exact SE value in DFT+U methods, strongly depends on the magnitude of the U and J parameters used^[25,40]. Therefore, regarding results from DFT+U+vdW methods, we mainly focus on the changes of J_{2D} values between two polymorphs.

Table 5. Band gaps, magnetic moments and J_{2D} values for AgF_2 and CuF_2 in $Pbca$ and $P2_1/c$ structures, obtained using various calculation methods. Negative values of J_{2D} indicate antiferromagnetic interaction.

Method	System	AgF_2			CuF_2		
		BG [eV]	$\pm\mu_{\text{AFM}}$	J_{2D} [meV]	BG [eV]	$\pm\mu_{\text{AFM}}$	J_{2D} [meV]
DFT+U	$Pbca$	2.18	0.66	-32.7	4.63	0.88	-6.6
	$P2_1/c$	1.95	0.67	-40.2	4.46	0.89	-8.2
DFT+U+vdW	$Pbca$	2.17	0.67	-31.9	4.64	0.88	-6.6
	$P2_1/c$	1.94	0.67	-39.4	4.46	0.89	-8.2
SCAN	$Pbca$	0.52	0.52	-67.3	1.58	0.75	-18.8
	$P2_1/c$	0.35	0.52	-81.0	1.21	0.76	-21.6
HSE06	$Pbca$	2.18	0.60	-54.7	4.46	0.81	-15.6
	$P2_1/c$	1.96	0.60	-63.2	4.14	0.81	-18.3

Calculations reveal enhancement of J_{2D} absolute values in AgF_2 in $P2_1/c$ forms by 13%-19%, depending on the method (**Table 5, Table S15**). This trend is also valid in the case of CuF_2 (13%-20%). Such changes of the J_{2D} value are strictly related to the changes of M-M distances, and linked to that, opening of the F-M-F angle driven by structural transformation $Pbca \rightarrow P2_1/c$. According to the GKA^[47-49] rules more effective overlapping of the orbitals should be expected with flattening of the F-M-F angle, and so, stronger hybridization of M-F orbitals leads to higher absolute value of antiferromagnetic J_{2D} . Since the J_{2D} value is related to the maximum experimental superconducting critical temperature in doped cuprates,^[50] synthesis of monoclinic AgF_2 precursor is worthwhile.

Another interesting aspect is the relationship between charge transfer energy and the J_{2D} value. For charge transfer insulators, hopping of electron from d orbital of transition metal site to another and back, engages p of nonmetal, thus J is proportional to $1/(\Delta_{\text{CT}})^2$ ^[47-49,51]. Indeed, our results show that larger $|J_{2D}|$ stems from smaller Δ_{CT} . This dependence is consistent within all methods employed (**Table 5, cf. ESI**), for both compounds in $Pbca$ and $P2_1/c$ structures.

Conclusions

In this paper, employing various theoretical methods, we investigated the structural, electronic and magnetic properties of the known, high-pressure orthorhombic form of CuF_2 ($Pbca$) and not-yet achieved monoclinic form of AgF_2 ($P2_1/c$), and compared them with those for ambient (p,T) polymorphs. Both fluorides are dynamically stable in the monoclinic structure and they exhibit higher $|J_{2D}|$ value, smaller charge-transfer gap and wider UHB, comparing to orthorhombic one. These findings are especially important in case of AgF_2 , which is perceived as analogue of cuprates. Stabilization of the monoclinic form of silver(II) difluoride ($P2_1/c$) may be crucial in order to achieving long-awaited doping of this compound.

Based on our theoretical results, we claim that the desired structural transition of AgF_2 to monoclinic form appears to be achievable in two possible ways (aside from partial Cu-doping^[25]): 1) at negative strain conditions^[43], or 2) upon heating to $T > 480$ K and quenching. Regarding 1), interatomic

Ag-Ag distance in AgF₂ layer may be controlled by lattice parameters of substrate, and thus ensuring proper strain for crystal growth of the P2₁/c polytype. Regarding 2), heating to 480 K should be accompanied by fluorine gas overpressure needed to prevent thermal decomposition. Regretfully, so far, such sudden thermal quenching experiments were not yet performed for AgF₂.

Acknowledgements

W.G. is grateful to the Polish National Science Center (NCN) for project Maestro (2017/26/A/ST5/00570). Research was carried out with the use of CePT infrastructure financed by the European Union – the European Regional Development Fund within the Operational Programme “Innovative economy” for 2007-2013 (POIG.02.02.00-14-024/08-00). Quantum mechanical calculations were performed using supercomputing resources of the ICM UW (projects SAPPHIRE GA83-34). Authors appreciate valuable comments from prof. Jose Lorenzana (CNR and La Sapienza, Rome, Italy).

Bibliography

- [1] W. H. Baur, S. Guggenheim, J. C. Lin, *Acta Crystallogr B Struct Crystallogr Cryst Chem* **1982**, *38*, 351–355.
- [2] J. W. Stout, S. A. Reed, *J. Am. Chem. Soc.* **1954**, *76*, 5279–5281.
- [3] A. Tressaud, J. L. Soubeyroux, H. Touhara, G. Demazeau, F. Langlais, *Materials Research Bulletin* **1981**, *16*, 207–214.
- [4] R. Maitland, K. Jack, *Proceedings of the Chemical Society* **1957**.
- [5] C. Billy, H. M. Haendler, *J. Am. Chem. Soc.* **1957**, *79*, 1049–1051.
- [6] P. Charpin, P. Plurien, P. Mériel, *Bulletin de Minéralogie* **1970**, *93*, 7–13.
- [7] L. Ming, M. H. Manghnani, *Geophysical Research Letters* **1978**, *5*, 491–494.
- [8] G. Liu, H. Wang, Y. Ma, Y. Ma, *Solid State Communications* **2011**, *151*, 1899–1902.
- [9] J. A. Barreda-Argüeso, S. López-Moreno, M. N. Sanz-Ortiz, F. Aguado, R. Valiente, J. González, F. Rodríguez, A. H. Romero, A. Muñoz, L. Nataf, F. Baudelet, *Phys. Rev. B* **2013**, *88*, 214108.
- [10] J. D. Jorgensen, T. G. Worlton, J. C. Jamieson, *Phys. Rev. B* **1978**, *17*, 2212–2214.
- [11] D. Kurzydłowski, *Crystals* **2018**, *8*, 140.
- [12] D. Kurzydłowski, A. Oleksiak, S. B. Pillai, P. K. Jha, *Inorg. Chem.* **2020**, *59*, 2584–2593.
- [13] A. Grzelak, J. Gawraczyński, T. Jaroń, D. Kurzydłowski, A. Budzianowski, Z. Mazej, P. J. Leszczyński, V. B. Prakapenka, M. Derzsi, V. V. Struzhkin, W. Grochala, *Inorg. Chem.* **2017**, *56*, 14651–14661.
- [14] S. Schyck, E. Evlyukhin, E. Kim, M. Pravica, *Chemical Physics Letters* **2019**, *724*, 35–41.
- [15] C. Kürkcü, Z. Merdan, H. Öztürk, *Russ. J. Phys. Chem.* **2016**, *90*, 2550–2555.
- [16] Z. Mazej, A. Tressaud, J. Darriet, *Journal of Fluorine Chemistry* **2001**, *110*, 139–143.
- [17] J. Gawraczyński, D. Kurzydłowski, R. A. Ewings, S. Bandaru, W. Gadomski, Z. Mazej, G. Ruani, I. Bergenti, T. Jaroń, A. Ozarowski, S. Hill, P. J. Leszczyński, K. Tokár, M. Derzsi, P. Barone, K. Wohlfeld, J. Lorenzana, W. Grochala, *Proc Natl Acad Sci USA* **2019**, *116*, 1495–1500.
- [18] R. Piombo, D. Jezierski, H. P. Martins, T. Jaroń, M. N. Gastiasoro, P. Barone, K. Tokár, P. Piekarczyk, M. Derzsi, Z. Mazej, M. Abbate, W. Grochala, J. Lorenzana, *Phys. Rev. B* **2022**, *106*, 035142.
- [19] N. Bachar, K. Koterias, J. Gawraczyński, W. Trzciński, J. Paszula, R. Piombo, P. Barone, Z. Mazej, G. Ghiringhelli, A. Nag, K.-J. Zhou, J. Lorenzana, D. Van Der Marel, W. Grochala, *Phys. Rev. Research* **2022**, *4*, 023108.
- [20] W. Grochala, R. Hoffmann, *Angew. Chem. Int. Ed.* **2001**, *40*, 2742–2781.
- [21] A. Grzelak, M. Derzsi, W. Grochala, *Inorg. Chem.* **2021**, *60*, 1561–1570.
- [22] S. Bandaru, M. Derzsi, A. Grzelak, J. Lorenzana, W. Grochala, *Phys. Rev. Materials* **2021**, *5*, 064801.
- [23] D. Jezierski, A. Grzelak, X. Liu, S. K. Pandey, M. N. Gastiasoro, J. Lorenzana, J. Feng, W. Grochala, *Phys. Chem. Chem. Phys.* **2022**, *24*, 15705–15717.
- [24] M. A. Domański, M. Derzsi, W. Grochala, *RSC Adv.* **2021**, *11*, 25801–25810.

- [25] D. Jezierski, K. Koterias, M. Domański, P. Połczyński, Z. Mazej, J. Lorenzana, W. Grochala, *Chemistry – A European Journal* **2023**, 29(52), e202301092.
- [26] G. Kresse, J. Furthmüller, *Phys. Rev. B* **1996**, 54, 11169–11186.
- [27] J. P. Perdew, A. Ruzsinszky, G. I. Csonka, O. A. Vydrov, G. E. Scuseria, L. A. Constantin, X. Zhou, K. Burke, *Phys. Rev. Lett.* **2008**, 100, 136406.
- [28] P. E. Blöchl, *Phys. Rev. B* **1994**, 50, 17953–17979.
- [29] G. Kresse, D. Joubert, *Phys. Rev. B* **1999**, 59, 1758–1775.
- [30] A. I. Liechtenstein, V. I. Anisimov, J. Zaanen, *Phys. Rev. B* **1995**, 52, R5467–R5470.
- [31] V. I. Anisimov, J. Zaanen, O. K. Andersen, *Phys. Rev. B* **1991**, 44, 943–954.
- [32] R. Piombo, D. Jezierski, H. P. Martins, T. Jaroń, M. N. Gastiasoro, P. Barone, K. Tokár, P. Piekarczyk, M. Derzsi, Z. Mazej, M. Abbate, W. Grochala, J. Lorenzana, *Phys. Rev. B* **2022**, 106, 035142.
- [33] A. B. Kunz, *Phys. Rev. B* **1982**, 26, 2070–2075.
- [34] S. Grimme, J. Antony, S. Ehrlich, H. Krieg, *The Journal of Chemical Physics* **2010**, 132, 154104.
- [35] A. Togo, I. Tanaka, *Scripta Materialia* **2015**, 108, 1–5.
- [36] P. Fischer, W. Hälg, D. Schwarzenbach, H. Gamsjäger, *Journal of Physics and Chemistry of Solids* **1974**, 35, 1683–1689.
- [37] K. Tokár, M. Derzsi, W. Grochala, *Computational Materials Science* **2021**, 188, 110250.
- [38] A. Jesih, K. Lutar, B. Žemva, B. Bachmann, St. Becker, B. G. Müller, R. Hoppe, *Z. Anorg. Allg. Chem.* **1990**, 588, 77–83.
- [39] W. Grochala, R. G. Egdell, P. P. Edwards, Z. Mazej, B. Žemva, *ChemPhysChem* **2003**, 4, 997–1001.
- [40] C. Miller, A. S. Botana, *Phys. Rev. B* **2020**, 101, 195116.
- [41] H. Eskes, G. A. Sawatzky, *Phys. Rev. Lett.* **1988**, 61, 1415–1418.
- [42] R. G. Pearson, *Acc. Chem. Res.* **1993**, 26, 250–255.
- [43] A. Grzelak, H. Su, X. Yang, D. Kurzydłowski, J. Lorenzana, W. Grochala, *Phys. Rev. Materials* **2020**, 4, 084405.
- [44] P. Fischer, G. Roullet, D. Schwarzenbach, *Journal of Physics and Chemistry of Solids* **1971**, 32, 1641–1647.
- [45] R. J. Joenk, R. M. Bozorth, *Journal of Applied Physics* **1965**, 36, 1167–1168.
- [46] P. Reinhardt, I. de P. R. Moreira, C. de Graaf, R. Dovesi, F. Illas, *Chemical Physics Letters* **2000**, 319, 625–630.
- [47] J. B. Goodenough, *Phys. Rev.* **1955**, 100, 564–573.
- [48] J. Kanamori, *Journal of Physics and Chemistry of Solids* **1959**, 10, 87–98.
- [49] P. W. Anderson, *Phys. Rev.* **1950**, 79, 350–356.
- [50] I. de P. R. Moreira, D. Muñoz, F. Illas, C. de Graaf, M. A. Garcia-Bach, *Chemical Physics Letters* **2001**, 345, 183–188.
- [51] D. I. Khomskii, *Transition Metal Compounds*, Cambridge University Press, **2014**.

SUPPLEMENTARY INFORMATION

Polymorphism of two-dimensional antiferromagnets, AgF_2 and CuF_2

Daniel Jezierski* and Wojciech Grochala*

*d.jezierski@cent.uw.edu.pl, w.grochala@cent.uw.edu.pl

Center of New Technologies, University of Warsaw, 020289 Warsaw Poland

List of contents

SI1. Pressure-induced phase transitions in TMF_2

SI2. Bond lengths for optimized $P2_1/c$ and $Pbca$ forms of AgF_2 and CuF_2

SI3. Thermodynamic data and superexchange constants for AgF_2 and CuF_2 in both structural forms

SI4. Phonon dispersion curves for $\text{AgF}_2/\text{CuF}_2$ in monoclinic and orthorhombic structures

SI5. Vibrational frequencies for $\text{AgF}_2/\text{CuF}_2$ in $P2_1/c$ and $Pbca$ forms

SI6. Electronic density of states for $\text{AgF}_2/\text{CuF}_2$ in $P2_1/c$ and $Pbca$ forms from HSE06 method

SI7 Optimized structures using all DFT methods

SI8. Bibliography

SI1. Pressure-induced phase transitions in TMF₂

Main types of structures:

1) Rutile:

- TiO₂ (*P4₂/mnm*) | tetragonal
- CaCl₂ (*Pnmm*) | orthorhombic
- distorted-rutile (*P2₁/c*) | monoclinic

2) Fluorite

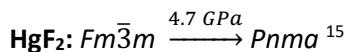
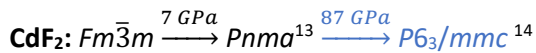
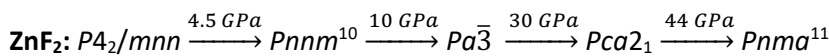
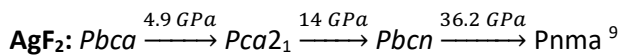
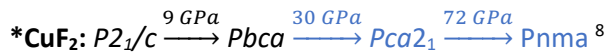
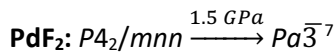
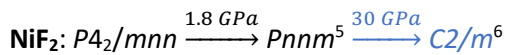
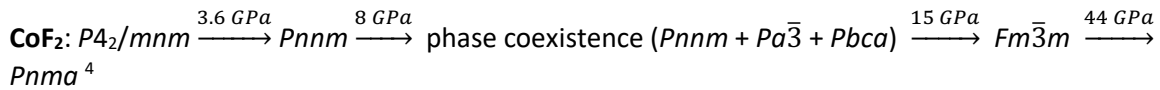
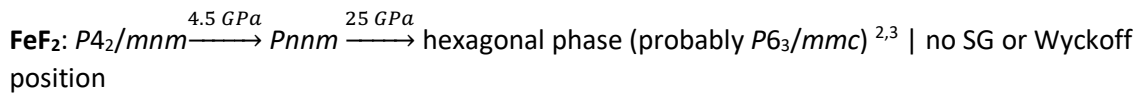
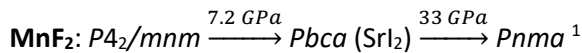
- HP-PdF₂ (*Pa $\bar{3}$*) | cubic
- CaF₂ (*Fm $\bar{3}m$*) | cubic
- distorted-fluorite (*Pbca*) | orthorhombic
- noncentrosymmetric (*Pca2₁*) | orthorhombic
- nanotubes (*Pbcn*) | orthorhombic

3) Cotunnite

- α -PbCl₂ (*Pnma*) | orthorhombic

4) Hexagonal

- Ni₂In (*P6₃/mmc*) | hexagonal



blue colour : DFT+U predictions

*CuF₂ compressed only up to 29.4 GPa. Theoretical prediction indicates, that the next structural transition should be around 30 GPa: *Pbca* -> *Pca2₁* (non-centrosymmetric).

SI2. Bond lengths for in optimized $P2_1/c$ and $Pbca$ forms of AgF_2 and CuF_2

Table SI1. Ag-F and Ag-Ag distances in AgF_2 compound in $P2_1/c$ and $Pbca$. Values in Å, based on fully optimized structures within all methods employed.

<i>Pbca</i>	d Ag-F [Å]				d Ag-Ag [Å]		
	in layer		apical	secondary	in layer	out layer	secondary
<i>DFT+U</i>	2.055	2.052	2.529	3.137	3.694	3.819	3.962
<i>DFT+U+vdW</i>	2.050	2.047	2.477	3.180	3.680	3.774	3.914
<i>SCAN</i>	2.087	2.089	2.570	3.135	3.798	3.850	3.998
<i>HSE06</i>	2.067	2.069	2.612	3.180	3.759	3.872	4.025
<i>P2₁/c</i>	in layer		apical	secondary	in layer	out layer	secondary
<i>DFT+U</i>	2.043	2.060	2.489	3.627	3.721	3.638	4.007
<i>DFT+U+vdW</i>	2.028	2.062	2.457	3.569	3.700	3.655	3.944
<i>SCAN</i>	2.075	2.095	2.546	3.687	3.810	3.743	4.025
<i>HSE06</i>	2.061	2.074	2.572	3.683	3.775	3.722	4.063

Table SI2. Cu-F and Cu-Cu distances in CuF_2 compound in $Pbca$ and $P2_1/c$ form. Values in Å, based on fully optimized structures within all methods employed.

<i>Pbca</i>	d Cu-F [Å]				dCu-Cu [Å]		
	in layer		apical	secondary	in layer	out layer	secondary
<i>DFT+U</i>	1.897	1.902	2.321	2.963	3.410	3.535	3.637
<i>DFT+U+vdW</i>	1.898	1.894	2.294	2.956	3.398	3.512	3.612
<i>SCAN</i>	1.904	1.910	2.403	3.020	3.442	3.590	3.712
<i>HSE06</i>	1.897	1.901	2.421	3.012	3.435	3.596	3.718
<i>P2₁/c</i>	in layer	apical	secondary	in layer	out layer	secondary	in layer
<i>DFT+U</i>	1.895	1.910	2.210	3.434	3.475	3.192	3.672
<i>DFT+U+vdW</i>	1.886	1.910	2.192	3.413	3.464	3.185	3.646
<i>SCAN</i>	1.899	1.919	2.302	3.442	3.487	3.302	3.740
<i>HSE06</i>	1.898	1.910	2.307	3.443	3.482	3.296	3.741

SI3. Thermodynamic data and superexchange constants for AgF_2 and CuF_2 in both structural forms

Table SI3. Ground state energy (GS energy), zero-point energies (ZPE), volumes of the unit cell (V), band gap values (BG), energy difference between AgF_2 in two systems (dE), volume difference of AgF_2 in two systems (dV) and the equilibrium pressure (p) for two AgF_2 systems – $Pbca$ and $P2_1/c$. $dE = E_{P2_1/c} - E_{Pbca}$ [meV], $dV = V_{Pbca} - V_{P2_1/c}$.

Structure	E/FU [eV]	V/FU [Å ³]	ZPE/FU [eV]	E with ZPE [eV]	dE [meV]	dE _{ZPE} [meV]	dV	p [GPa]	p _{ZPE} [GPa]	BG [eV]
<i>DFT+U, U = 8 eV</i>										
<i>Pbca</i>	-8.806	39.233	0.125	-8.681	-2.338	-8.234	-2.774	0.1	0.5	2.18
<i>P2₁/c</i>	-8.808	42.006	0.119	-8.689						1.95
<i>DFT + U + vdW, U = 8 eV</i>										
<i>Pbca</i>	-9.273	38.211	0.129	-9.144	49.383	41.404	-2.785	-2.8	-2.4	2.17
<i>P2₁/c</i>	-9.224	40.995	0.121	-9.103						1.94
<i>SCAN</i>										
<i>Pbca</i>	-127.382	41.145	0.123	-127.259	36.635	15.880	-3.031	-1.9	-0.8	0.52
<i>P2₁/c</i>	-127.345	44.176	0.102	-127.243						0.35
<i>HSE06</i>										
<i>Pbca</i>	-13.491	41.071	0.126	-13.366	3.707	-2.167	-2.779	-0.2	0.1	2.18
<i>P2₁/c</i>	-13.488	43.850	0.120	-13.368						1.96

Table S14. Ground state energy (GS energy), zero-point energies (ZPE), volumes of unit cell (V), band gap values (BG), energy difference between CuF_2 in two systems (dE), volume difference of AgF_2 in two systems (dV) and the equilibrium pressure (p) for two CuF_2 systems – *Pbca* and *P21/c*. $dE = E_{Pbca} - E_{P21/c}$ [meV], $dV = V_{P21/c} - V_{Pbca}$

Structure	E/FU [ev]	V/FU [\AA^3]	ZPE/FU [eV]	E with ZPE [ev]	dE [meV]	dE _{ZPE} [meV]	dV	p [GPa]	p _{ZPE} [GPa]	BG [eV]
<i>DFT+U, U = 10 eV</i>										
<i>Pbca</i>	-11.165	30.803	0.150	-11.015	102.837	112.432	1.706	9.7	10.6*	4.63
<i>P21/c</i>	-11.268	32.510	0.140	-11.128						4.46
<i>DFT + U + vdW, U = 10 eV</i>										
<i>Pbca</i>	-11.557	30.311	0.154	-11.403	69.358	80.423	1.756	6.3	7.3	4.64
<i>P21/c</i>	-11.626	32.068	0.143	-11.483						4.46
<i>SCAN</i>										
<i>Pbca</i>	-80.825	32.154	0.145	-80.680	40.923	52.928	1.763	3.7	4.8	1.58
<i>P21/c</i>	-80.866	33.917	0.133	-80.733						1.21
<i>HSE06</i>										
<i>Pbca</i>	-16.241	32.073	0.154	-16.087	65.676	76.914	1.650	6.4	7.5	4.46
<i>P21/c</i>	-16.307	33.724	0.143	-16.164						4.14

* transition at 9GPa reported experimentally by Kurzydłowski⁸

Table S15. J_{2D} [meV] value for AgF_2 and CuF_2 in two types of structure: *P21/c* and *Pbca* calculated using four methods: DFT+U, DFT+U+vdW, SCAN, HSE06. F-Ag-F angles for in-layer plaquettes.

Method	J_{2D} [meV]									
	AgF_2					CuF_2				
	<i>Pbca</i>	F-Ag-F angle [°]	<i>P21/c</i>	F-Ag-F angle [°]	$J_{Pbca}/J_{P21/c}$	<i>Pbca</i>	F-Ag-F angle [°]	<i>P21/c</i>	F-Ag-F angle [°]	$J_{Pbca}/J_{P21/c}$
DFT+U	-32.7	128.2	-40.7	130.1	0.81	-6.6	127.7	-8.2	132.0	0.81
DFT+U+vdW	-31.9	127.9	-39.4	129.5	0.81	-6.6	127.3	-8.2	131.7	0.80
SCAN	-67.3	130.8	-81.0	132.0	0.83	-18.8	128.9	-21.6	131.9	0.87
HSE06	-52.0	130.6	-59.1	131.8	0.87	-15.6	129.4	-18.3	132.2	0.85

S14. Optimized structure following imaginary mode

Table S16. Parameters of unit cells obtained after optimization of the specific displacement, following imaginary mode. The symmetry of the optimized structure (marked as i-mode) was found using Materials Studio software.

Parameters	CuF_2		AgF_2	
	i-mode (<i>P21/c</i>)	<i>P21/c</i>	i-mode (<i>P21/c</i>)	<i>P21/c</i>
a [\AA]	4.543	3.192	4.871	3.638
b [\AA]	4.504	4.505	4.775	4.777
c [\AA]	4.800	5.293	6.428	5.706
alpha [°]	90.000	90.000	90.000	90.000
beta [°]	146.784	122.091	145.848	122.091
gamma [°]	90.000	90.000	90.000	90.000
V/FU [\AA^3]	32.503	32.510	41.965	42.006
E/FU [eV]	-11.268	-11.268	-8.808	-8.808
$E_{diff} (E_{i-mode} - E_{P21/c})$ [meV]	-0.113		-0.105	

Imaginary mode for AgF_2 and CuF_2 , both in the *P21/c* structure, with minimum around Gamma point $q = (-0.04, 0.04, -0.04)$. Frequency of minimum point: -8.387 cm^{-1} and -10.464 cm^{-1} for AgF_2 and CuF_2 , respectively.

Optimized structures are ca. -0.1 meV lower in energy from parent structures, which is v -within error bar of the DFT method, and strongly suggests that imaginary character of the phonon is **artificial**.

S15. Vibrational frequencies for AgF₂/CuF₂ in P2₁/c and Pbcu forms

Table S17. Phonon frequencies for AgF₂ and CuF₂ in Pbcu systems (DFT+U). The last three bands correspond to the translations. For CuF₂ theoretical frequencies were assigned to the experimental values, with classification of the modes based on the relative intensity: shoulder (sh), very strong (vs), strong (s), medium (m) and weak (w).

Pbcu				P2 ₁ /c				EXP CuF ₂ only*
#	AgF ₂ *	CuF ₂	Symm.	#	AgF ₂	CuF ₂	Symm.	
1	472	523	B _{1g} (RAMAN)	1	486	551	B _g (RAMAN)	556 (w)
2	469	520	B _{2g} (RAMAN)	2	450	493	A _u (IR)	508 (sh)
3	465	523	A _u (silent)	3	447	482	B _u (IR)	483 (vs)
4	457	504	B _{1u} (IR)	4	341	380	A _g (RAMAN)	355 (m)
5	456	513	B _{3u} (IR)	5	322	363	A _u (IR)	360 (sh)
6	441	473	B _{2u} (IR)	6	319	351	B _u (IR)	354 (s)
7	361	427	B _{2u} (IR)	7	242	258	A _g (RAMAN)	254 (s)
8	334	385	A _u (silent)	8	237	292	B _g (RAMAN)	293 (vs)
9	330	386	B _{3g} (RAMAN)	9	183	246	B _u (IR)	243 (s)
10	320	366	B _{1u} (IR)	10	180	232	B _g (RAMAN)	221 (s)
11	318	366	B _{3u} (IR)	11	176	247	A _u (IR)	246 (s)
12	313	360	B _{3g} (RAMAN)	12	167	220	A _u (IR)	220 (sh)
13	308	349	A _g (RAMAN)	13	145	188	B _u (IR)	190 (s)
14	264	312	B _{1g} (RAMAN)	14	103	140	A _u (IR)	136 (m)
15	263	345	B _{2g} (RAMAN)	15	48	84	A _g (RAMAN)	n.d.
16	234	238	A _g (RAMAN)	16	0	1	B _u	
17	195	261	B _{3u} (IR)	17	1	2	A _u	
18	191	255	B _{1u} (IR)	18	1	2	B _u	
19	188	248	A _u (silent)					
20	181	274	B _{1g} (RAMAN)					
21	168	229	A _u (silent)					
22	166	236	B _{2u} (IR)					
23	158	198	B _{2u} (IR)					
24	146	167	B _{3u} (IR)					
25	139	154	B _{1u} (IR)					
26	136	153	B _{2g} (RAMAN)					
27	127	217	B _{3g} (RAMAN)					
28	102	157	A _u (silent)					
29	97	126	B _{2u} (IR)					
30	91	113	B _{3u} (IR)					
31	75	91	A _u (silent)					
32	69	66	A _g (RAMAN)					
33	35	54	B _{1u} (IR)					
34	0	1	B _{2u}					
35	0	1	B _{1u}					
36	1	2	B _{3u}					

* experimental data published by Gawraczyński et.al, PNAS 2019¹⁶, ** for RAMAN data taken from Kurzydłowski⁸, for IR own results.

Table S18. Phonon frequencies for AgF₂ in *Pbca* system for all methods. The last three bands correspond to the translations.

#	DFT+U		DFT+U+vdw		SCAN		HSE06	
	cm ⁻¹	Symm.						
1	472	B _{1g}	478	B _{1g}	476	A _u	480	B _{1g}
2	469	B _{2g}	475	B _{2g}	468	B _{3u}	477	B _{2g}
3	465	A _u	473	A _u	467	B _{1u}	475	A _u
4	457	B _{1u}	467	B _{1u}	451	B _{2u}	469	B _{1u}
5	456	B _{3u}	464	B _{3u}	414	B _{1g}	467	B _{3u}
6	441	B _{2u}	450	B _{2u}	411	B _{2g}	458	B _{2u}
7	361	B _{2u}	369	B _{2u}	343	B _{2u}	355	B _{2u}
8	334	A _u	347	A _u	326	B _{3g}	343	B _{3g}
9	330	B _{3g}	332	B _{3g}	317	A _u	329	A _g
10	320	B _{1u}	329	B _{1u}	311	A _g	325	A _u
11	318	B _{3u}	325	B _{3u}	304	B _{1u}	318	B _{3u}
12	313	B _{3g}	324	B _{3g}	302	B _{3g}	318	B _{1u}
13	308	A _g	307	A _g	301	B _{3u}	306	B _{3g}
14	264	B _{1g}	274	B _{1g}	252	B _{1g}	257	B _{1g}
15	263	B _{2g}	273	B _{2g}	249	B _{2g}	250	B _{2g}
16	234	A _g	240	A _g	225	A _g	232	A _g
17	195	B _{3u}	203	B _{3u}	212	A _u	196	B _{1u}
18	191	B _{1u}	197	B _{1u}	207	B _{1u}	193	A _u
19	188	A _u	191	A _u	204	B _{3u}	193	B _{3u}
20	181	B _{1g}	186	B _{1g}	184	B _{1g}	179	B _{1g}
21	168	A _u	172	A _u	174	B _{2u}	173	B _{2u}
22	166	B _{2u}	172	B _{2u}	168	B _{2u}	168	A _u
23	158	B _{2u}	165	B _{2u}	159	A _u	160	B _{2u}
24	146	B _{3u}	148	B _{3u}	139	B _{3g}	141	B _{3u}
25	139	B _{1u}	148	B _{1u}	134	B _{2g}	137	B _{1u}
26	136	B _{2g}	137	B _{2g}	132	B _{3u}	135	B _{2g}
27	127	B _{3g}	136	B _{3g}	123	B _{1u}	119	B _{3g}
28	102	A _u	114	A _u	116	A _u	102	A _u
29	97	B _{2u}	105	B _{2u}	88	A _g	96	B _{3u}
30	91	B _{3u}	99	B _{3u}	83	B _{2u}	95	B _{2u}
31	75	A _u	90	A _u	65	B _{1u}	76	A _u
32	69	A _g	79	A _g	64	B _{3u}	68	A _g
33	35	B _{1u}	45	B _{1u}	44	A _u	31	B _{1u}
34	0	B _{2u}	0	B _{2u}	15	B _{3u}	1	B _{2u}
35	0	B _{1u}	1	B _{1u}	24	B _{2u}	2	B _{3u}
36	1	B _{3u}	1	B _{3u}	29	B _{1u}	3	B _{1u}

Table S19. Phonon frequencies for CuF₂ in *Pbca* system for all methods. The last three bands correspond to the translations.

#	DFT+U		DFT+U+vdw		SCAN		HSE06	
	cm ⁻¹	Symm.						
1	523	A _u	528	A _u	527	A _u	559	B _{1g}
2	523	B _{1g}	526	B _{1g}	518	B _{3u}	555	B _{2g}
3	520	B _{2g}	524	B _{2g}	512	B _{1u}	544	A _u
4	513	B _{3u}	518	B _{3u}	490	B _{2u}	536	B _{3u}
5	504	B _{1u}	511	B _{1u}	476	B _{2g}	528	B _{1u}
6	473	B _{2u}	476	B _{2u}	475	B _{1g}	507	B _{2u}
7	427	B _{2u}	432	B _{2u}	410	B _{2u}	437	B _{2u}
8	386	B _{3g}	395	A _u	375	A _u	393	A _u
9	385	A _u	388	B _{3g}	374	B _{3g}	391	B _{3u}
10	366	B _{3u}	372	B _{1u}	372	B _{3u}	391	B _{3g}
11	366	B _{1u}	371	B _{3u}	369	B _{1u}	388	B _{1u}
12	360	B _{3g}	369	B _{3g}	348	A _g	363	A _g
13	349	A _g	357	B _{2g}	315	B _{3g}	355	B _{3g}
14	345	B _{2g}	347	A _g	314	B _{2g}	337	B _{2g}
15	312	B _{1g}	318	B _{1g}	293	B _{1g}	315	B _{1g}
16	274	B _{1g}	283	B _{1g}	243	B _{1g}	263	B _{3u}
17	261	B _{3u}	267	B _{3u}	241	B _{1u}	260	B _{1g}
18	255	B _{1u}	261	B _{1u}	241	B _{3u}	259	B _{1u}
19	248	A _u	254	A _u	235	A _g	256	A _g
20	238	A _g	242	A _g	232	A _u	247	A _u
21	236	B _{2u}	241	B _{2u}	225	B _{2u}	235	B _{2u}
22	229	A _u	231	A _u	216	A _u	234	A _u
23	217	B _{3g}	231	B _{3g}	200	B _{2u}	211	B _{2u}
24	198	B _{2u}	203	B _{2u}	187	B _{3g}	198	B _{3g}
25	167	B _{3u}	180	A _g	163	B _{3u}	174	B _{3u}
26	166	A _g	172	B _{3u}	158	B _{1u}	165	B _{1u}
27	157	A _u	160	A _u	143	B _{2g}	156	B _{2g}
28	154	B _{1u}	160	B _{1u}	142	A _g	151	A _u
29	153	B _{2g}	157	B _{2g}	140	A _u	150	A _g
30	126	B _{2u}	141	B _{2u}	127	B _{2u}	125	B _{3u}
31	113	B _{3u}	120	B _{3u}	123	B _{3u}	124	B _{2u}
32	91	A _u	104	A _u	100	A _u	96	A _u
33	54	B _{1u}	71	B _{1u}	49	B _{1u}	56	B _{1u}
34	1	B _{2u}	1	B _{3u}	1	B _{2u}	1	B _{1u}
35	1	B _{1u}	1	B _{2u}	3	B _{3u}	2	B _{2u}
36	2	B _{3u}	2	B _{1u}	4	B _{1u}	2	B _{3u}

Table SI10. Phonon frequencies for AgF_2 in $P2_1/c$ system for all methods. The last three bands correspond to the translations.

#	DFT+U		DFT+U+vdW		SCAN		HSE06	
	cm^{-1}	Symm.	cm^{-1}	Symm.	cm^{-1}	Symm.	cm^{-1}	Symm.
1	486	B_g	493	B_g	458	A_u	487	B_g
2	450	A_u	453	B_u	455	B_u	463	A_u
3	447	B_u	452	A_u	324	A_g	460	B_u
4	341	A_g	355	A_g	276	A_u	348	A_g
5	322	A_u	333	A_u	270	B_g	316	A_u
6	319	B_u	326	B_u	257	B_u	316	B_u
7	242	A_g	241	B_g	208	A_g	239	A_g
8	237	B_g	240	A_g	183	B_u	233	B_g
9	183	B_u	183	B_u	183	B_g	188	B_u
10	180	B_g	180	A_u	180	A_u	178	B_g
11	176	A_u	175	B_g	130	B_g	178	A_u
12	167	A_u	158	A_u	109	A_u	165	A_u
13	145	B_u	149	B_u	96	B_u	140	B_u
14	103	A_u	108	A_u	94	A_u	103	A_u
15	48	A_g	54	A_g	63	A_g	59	A_g
16	0	B_u	0	B_u	0	B_u	0	B_u
17	1	A_u	0	A_u	0	B_u	0	A_u
18	1	B_u	1	B_u	1	A_u	2	B_u

Table SI11. Phonon frequencies for CuF_2 in $P2_1/c$ system for all methods. The last three bands correspond to the translations.

#	DFT+U		DFT+U+vdW		SCAN		HSE06	
	cm^{-1}	Symm.	cm^{-1}	Symm.	cm^{-1}	Symm.	cm^{-1}	Symm.
1	551	B_g	560	B_g	503	A_u	575	B_g
2	493	A_u	500	A_u	495	B_u	518	A_u
3	482	B_u	490	B_u	492	B_g	508	B_u
4	380	A_g	389	A_g	371	A_g	379	A_g
5	363	A_u	373	A_u	362	A_u	377	A_u
6	351	B_u	357	B_u	349	B_u	372	B_u
7	292	B_g	294	B_g	266	B_g	291	B_g
8	258	A_g	263	A_g	237	A_g	267	A_g
9	247	A_u	254	A_u	229	B_u	245	B_u
10	246	B_u	250	B_u	215	A_u	236	A_u
11	232	B_g	235	B_g	208	A_u	227	B_g
12	220	A_u	220	A_u	198	B_g	227	A_u
13	188	B_u	192	B_u	167	B_u	185	B_u
14	140	A_u	145	A_u	127	A_u	138	A_u
15	84	A_g	75	A_g	59	A_g	77	A_g
16	1	B_u	0	B_u	1	A_u	1	B_u
17	2	A_u	1	B_u	1	B_u	1	A_u
18	2	B_u	2	A_u	1	B_u	2	B_u

SI6. Electronic density of states for $\text{AgF}_2/\text{CuF}_2$ in $P2_1/c$ and $Pbca$ forms from HSE06 method

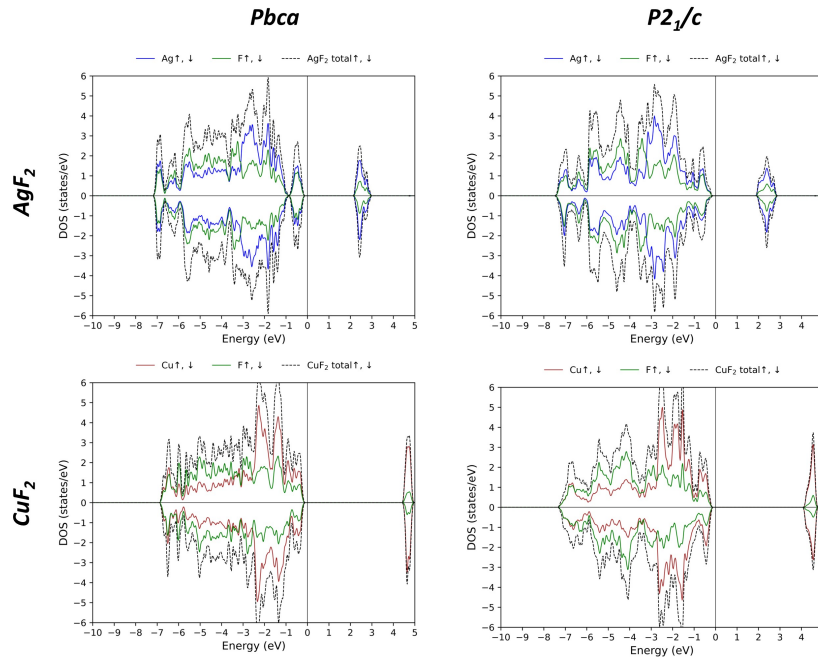


Fig. SI1 Atom-resolved density of states for AgF_2 and CuF_2 in both crystal structures, within HSE06 method.

SI7 Optimized structures from SCAN method

$\text{AgF}_2_Pbca_DFT+U$

5.4325827684372898	0.0000000000000000	0.0000000000000000
0.0000000000000000	5.7683784010416890	0.0000000000000000
0.0000000000000000	0.0000000000000000	5.0079337523618577

Ag F
4 8

Direct

-0.0000000000000000	-0.0000000000000000	-0.0000000000000000
0.5000000000000000	-0.0000000000000000	0.5000000000000000
-0.0000000000000000	0.5000000000000000	0.5000000000000000
0.5000000000000000	0.5000000000000000	-0.0000000000000000
0.3081704282328906	0.8672726819052461	0.1810474953492010
0.6918295717671094	0.1327272890947479	0.8189525046507991
0.1918295717671094	0.1327272890947479	0.6810474953492009
0.8081704282328906	0.8672726819052461	0.3189525046507990
0.6918295717671094	0.3672727109052521	0.3189525046507990
0.3081704282328906	0.6327273180947539	0.6810474953492009
0.8081704282328906	0.6327273180947539	0.8189525046507991
0.1918295717671094	0.3672727109052521	0.1810474953492010

$\text{AgF}_2_Pbca_DFT+U+vdW$

5.4084161242709152	0.0000000000000000	0.0000000000000000
0.0000000000000000	5.6604891530796744	0.0000000000000000
-0.0000000000000000	0.0000000000000000	4.9925371834847416

Ag F

4 8

Direct

-0.0000000000000000 -0.0000000000000000 -0.0000000000000000
0.5000000000000000 -0.0000000000000000 0.5000000000000000
-0.0000000000000000 0.5000000000000000 0.5000000000000000
0.5000000000000000 0.5000000000000000 -0.0000000000000000
0.3112495951615513 0.8666956753121100 0.1776014607481890
0.6887504048384488 0.1333042956878842 0.8223985392518115
0.1887504048384489 0.1333042956878842 0.6776014607481885
0.8112495951615512 0.8666956753121100 0.3223985392518112
0.6887504048384488 0.3666957043121157 0.3223985392518112
0.3112495951615513 0.6333043246878900 0.6776014607481885
0.8112495951615512 0.6333043246878900 0.8223985392518115
0.1887504048384489 0.3666957043121157 0.1776014607481890

AgF₂_Pbca_SCAN

5.5825253940946036 0.0000000000000000 0.0000000000000000
0.0000000000000000 5.7238028965063732 0.0000000000000000
0.0000000000000000 0.0000000000000000 5.1506410134567648

Ag F

4 8

Direct

-0.0000000000000000 -0.0000000000000000 0.0000000000000000
0.5000000000000000 -0.0000000000000000 0.5000000000000000
-0.0000000000000000 0.5000000000000000 0.5000000000000000
0.5000000000000000 0.5000000000000000 0.0000000000000000
0.3018553765971723 0.8676807184337415 0.1894365447265209
0.6981446234028278 0.1323192525662527 0.8105634552734791
0.1981446234028275 0.1323192525662527 0.6894365447265209
0.8018553765971722 0.8676807184337415 0.3105634552734791
0.6981446234028278 0.3676807474337472 0.3105634552734791
0.3018553765971723 0.6323192815662585 0.6894365447265209
0.8018553765971722 0.6323192815662585 0.8105634552734791
0.1981446234028275 0.3676807474337472 0.1894365447265210

AgF₂_Pbca_HSE06

5.5385447024405279 0.0000000000000000 -0.0000000000000000
0.0000000000000000 5.8425028417607319 0.0000000000000000
-0.0000000000000000 0.0000000000000000 5.0823121733048504

Ag F

4 8

Direct

0.0000000000000000 -0.0000000000000000 -0.0000000000000000
0.5000000000000000 -0.0000000000000000 0.5000000000000000
0.0000000000000000 0.5000000000000000 0.5000000000000000
0.5000000000000000 0.5000000000000000 -0.0000000000000000
0.3035307753632584 0.8727315986283707 0.1861317494483685
0.6964692246367415 0.1272683723716233 0.8138682505516314
0.1964692246367415 0.1272683723716233 0.6861317494483686
0.8035307753632585 0.8727315986283707 0.3138682505516315
0.6964692246367415 0.3727316276283767 0.3138682505516315
0.3035307753632584 0.6272684013716293 0.6861317494483686
0.8035307753632585 0.6272684013716293 0.8138682505516314

0.1964692246367415 0.3727316276283767 0.1861317494483685

AgF₂_P2₁/c_DFT+U

3.6384468137734780 0.0000000000000000 -0.0041520798417513
0.0000000000000000 4.7768034691478833 0.0000000000000000
-3.0257122287743710 0.0000000000000000 4.8372583721165396

Ag F
2 4

Direct

0.0000000000000000 -0.0000000000000000 0.0000000000000000
0.0000000000000000 0.5000000000000000 0.5000000000000000
0.2580612161134505 0.3032513596006569 0.2979143887080884
0.7419387838865490 0.6967486113993373 0.7020856402919100
0.7419387838865490 0.8032513886006627 0.2020856112919114
0.2580612161134505 0.1967486403993431 0.7979143597080900

AgF₂_P2₁/c_DFT+U+vdW

3.6578695608297194 0.0000000000000000 -0.0449210475348461
0.0000000000000000 4.7214582353131362 0.0000000000000000
-3.0965754060751922 0.0000000000000000 4.7800051707746958

Ag F
2 4

Direct

0.0000000000000000 -0.0000000000000000 0.0000000000000000
0.0000000000000000 0.5000000000000000 0.5000000000000000
0.2601460237587488 0.3070580012521441 0.2989172378806293
0.7398539762412513 0.6929419697478429 0.7010827911193696
0.7398539762412513 0.8070580302521571 0.2010827621193707
0.2601460237587488 0.1929419987478489 0.7989172088806304

AgF₂_P2₁/c_SCAN

3.7415840779467833 0.0000000000000000 -0.0918547643182602
0.0000000000000000 4.9088817666584550 0.0000000000000000
-3.1729438680646593 0.0000000000000000 4.8882392413909601

Ag F
2 4

Direct

-0.0000000000000000 -0.0000000000000000 -0.0000000000000000
-0.0000000000000000 0.5000000000000000 0.5000000000000000
0.2460597954672760 0.3072026777366762 0.2961816016485471
0.7539402045327240 0.6927972932633180 0.7038184273514519
0.7539402045327240 0.8072027067366820 0.2038183983514530
0.2460597954672760 0.1927973222633238 0.7961815726485481

AgF₂_P2₁/c_HSE06

3.7170509955380622 0.0000000000000000 0.0047660820843200
0.0000000000000000 4.8239178583612023 0.0000000000000000
-3.0792251184526580 0.0000000000000000 4.8870756396050909

Ag F
2 4

Direct

0.0000000000000000 -0.0000000000000000 -0.0000000000000000
0.0000000000000000 0.5000000000000000 0.5000000000000000
0.2505233569641341 0.3029229041044571 0.2967999047589231
0.7494766430358657 0.6970770668955373 0.7032001242410757
0.7494766430358657 0.8029229331044627 0.2032000952410770
0.2505233569641341 0.1970770958955429 0.7967998757589243

CuF₂_Pbca_DFT+U

4.9711335115512245 0.0000000000000000 -0.0000000000000000
0.0000000000000000 5.3097794773679450 0.0000000000000000
0.0000000000000000 0.0000000000000000 4.6679476639154105

Cu F

4 8

Direct

-0.0000000000000000 -0.0000000000000000 -0.0000000000000000
0.5000000000000000 -0.0000000000000000 0.5000000000000000
-0.0000000000000000 0.5000000000000000 0.5000000000000000
0.5000000000000000 0.5000000000000000 -0.0000000000000000
0.3183095129465213 0.8732020347780225 0.1717660482612136
0.6816904870534715 0.1267979362219716 0.8282339517387864
0.1816904870534716 0.1267979362219716 0.6717660482612136
0.8183095129465285 0.8732020347780225 0.3282339517387864
0.6816904870534715 0.3732020637780284 0.3282339517387864
0.3183095129465213 0.6267979652219775 0.6717660482612136
0.8183095129465285 0.6267979652219775 0.8282339517387864
0.1816904870534716 0.3732020637780284 0.1717660482612136

CuF₂_Pbca_DFT+U+vdW

4.9511571524161839 0.0000000000000000 -0.0000000000000000
0.0000000000000000 5.2592024115207971 0.0000000000000000
-0.0000000000000000 0.0000000000000000 4.6562936912203581

Cu F

4 8

Direct

-0.0000000000000000 0.0000000000000000 0.0000000000000000
0.5000000000000000 0.0000000000000000 0.5000000000000000
-0.0000000000000000 0.5000000000000000 0.5000000000000000
0.5000000000000000 0.5000000000000000 0.0000000000000000
0.3206705495773565 0.8731719024696725 0.1695527903438375
0.6793294504226364 0.1268280685303217 0.8304472096561626
0.1793294504226365 0.1268280685303217 0.6695527903438374
0.8206705495773636 0.8731719024696725 0.3304472096561625
0.6793294504226364 0.3731719314696783 0.3304472096561625
0.3206705495773565 0.6268280975303275 0.6695527903438374
0.8206705495773636 0.6268280975303275 0.8304472096561626
0.1793294504226365 0.3731719314696783 0.1695527903438375

CuF₂_Pbca_SCAN

5.0470466179036055 0.0000000000000000 -0.0000000000000000
0.0000000000000000 5.4448582294964751 0.0000000000000000
0.0000000000000000 0.0000000000000000 4.6802399712243048

Cu F
4 8

Direct

0.0000000000000000	-0.0000000000000000	0.0000000000000000
0.5000000000000000	-0.0000000000000000	0.5000000000000000
0.0000000000000000	0.5000000000000000	0.5000000000000000
0.5000000000000000	0.5000000000000000	0.0000000000000000
0.3152406344036440	0.8784445413341972	0.1731180155087471
0.6847593655963489	0.1215554296657968	0.8268819844912528
0.1847593655963489	0.1215554296657968	0.6731180155087472
0.8152406344036511	0.8784445413341972	0.3268819844912529
0.6847593655963489	0.3784445703342033	0.3268819844912529
0.3152406344036440	0.6215554586658028	0.6731180155087472
0.8152406344036511	0.6215554586658028	0.8268819844912527
0.1847593655963489	0.3784445703342033	0.1731180155087471

CuF₂_Pbca_HSE06

5.0375200457129949	0.0000000000000000	0.0000000000000000
0.0000000000000000	5.4703986051368156	0.0000000000000000
-0.0000000000000000	0.0000000000000000	4.6703820614650837

Cu F
4 8

Direct

-0.0000000000000000	0.0000000000000000	0.0000000000000000
0.5000000000000000	0.0000000000000000	0.5000000000000000
0.0000000000000000	0.5000000000000000	0.5000000000000000
0.5000000000000000	0.5000000000000000	0.0000000000000000
0.3129443861067328	0.8788919183021422	0.1760803685437572
0.6870556138932602	0.1211080526978519	0.8239196314562428
0.1870556138932601	0.1211080526978519	0.6760803685437572
0.8129443861067398	0.8788919183021422	0.3239196314562429
0.6870556138932602	0.3788919473021410	0.3239196314562429
0.3129443861067328	0.6211080816978578	0.6760803685437572
0.8129443861067398	0.6211080816978578	0.8239196314562428
0.1870556138932601	0.3788919473021410	0.1760803685437572

CuF₂_P2₁/c_DFT+U

3.1918032843702164	0.0000000000000000	-0.0282795905905217
0.0000000000000000	4.5049849400793818	0.0000000000000000
-2.7117339860874119	0.0000000000000000	4.5458609099431406

Cu F
2 4

Direct

0.0000000000000000	0.0000000000000000	0.0000000000000000
0.0000000000000000	0.5000000000000000	0.5000000000000000
0.2633370751632447	0.2980220513899945	0.2958083607980840
0.7366629248367553	0.7019779196100067	0.7041916682019148
0.7366629248367553	0.7980220803899933	0.2041916392019160
0.2633370751632447	0.2019779486100055	0.7958083317980852

CuF₂_P2₁/c_DFT+U+vdW

3.1843616963673211	0.0000000000000000	-0.0401347544237979
--------------------	--------------------	---------------------

0.0000000000000000 4.4787430856724946 0.0000000000000000
-2.7224144821479328 0.0000000000000000 4.5312785681204444

Cu F
2 4

Direct

0.0000000000000000 -0.0000000000000000 0.0000000000000000
0.0000000000000000 0.5000000000000000 0.5000000000000000
0.2650117692506215 0.2983719618346402 0.2960198521911562
0.7349882307493785 0.7016280091653607 0.7039801768088426
0.7349882307493785 0.7983719908346393 0.2039801478088439
0.2650117692506215 0.2016280381653597 0.7960198231911574

CuF₂_P2₁/c_SCAN

3.3024484670833067 0.0000000000000000 0.0040032864862328
0.0000000000000000 4.5224078706716684 0.0000000000000000
-2.7558793437961513 0.0000000000000000 4.5385905413277614

Cu F
2 4

Direct

0.0000000000000000 0.0000000000000000 -0.0000000000000000
0.0000000000000000 0.5000000000000000 0.5000000000000000
0.2544117004725763 0.2984925719792934 0.2940252647869827
0.7455882995274238 0.7015073990207077 0.7059747642130163
0.7455882995274238 0.7984926009792923 0.2059747352130173
0.2544117004725763 0.2015074280207066 0.7940252357869837

CuF₂_P2₁/c_HSE06

3.2956089918571907 0.0000000000000000 0.0114348804553170
0.0000000000000000 4.5164592600711346 0.0000000000000000
-2.7434020870818063 0.0000000000000000 4.5343499734704871

Cu F
2 4

Direct

-0.0000000000000000 0.0000000000000000 -0.0000000000000000
-0.0000000000000000 0.5000000000000000 0.5000000000000000
0.2530356795178663 0.2976717097460082 0.2947272241957566
0.7469643204821337 0.7023282612539932 0.7052728048042424
0.7469643204821337 0.7976717387460068 0.2052727758042435
0.2530356795178663 0.2023282902539919 0.7947271951957576

SI8. Bibliography

- (1) Stavrou, E.; Yao, Y.; Goncharov, A. F.; Konôpková, Z.; Raptis, C. High-Pressure Structural Study of MnF₂. *Phys. Rev. B* **2016**, *93* (5), 054101. <https://doi.org/10.1103/PhysRevB.93.054101>.
- (2) Ming, L.; Manghnani, M. H. High Pressure Phase Transformation in FeF₂ (Rutile). *Geophysical Research Letters* **1978**, *5* (6), 491–494. <https://doi.org/10.1029/GL005i006p00491>.
- (3) Wang, H.; Liu, X.; Li, Y.; Liu, Y.; Ma, Y. First-Principles Study of Phase Transitions in Antiferromagnetic (Fe, Co and Ni). *Solid State Communications* **2011**, *151* (20), 1475–1478. <https://doi.org/10.1016/j.ssc.2011.06.036>.
- (4) Barreda-Argüeso, J. A.; López-Moreno, S.; Sanz-Ortiz, M. N.; Aguado, F.; Valiente, R.; González, J.; Rodríguez, F.; Romero, A. H.; Muñoz, A.; Nataf, L.; Baudelet, F. Pressure-Induced Phase-Transition

- Sequence in CoF_2 : An Experimental and First-Principles Study on the Crystal, Vibrational, and Electronic Properties. *Phys. Rev. B* **2013**, *88* (21), 214108. <https://doi.org/10.1103/PhysRevB.88.214108>.
- (5) Jorgensen, J. D.; Worlton, T. G.; Jamieson, J. C. Pressure-Induced Strain Transition in NiF_2 . *Phys. Rev. B* **1978**, *17* (5), 2212–2214. <https://doi.org/10.1103/PhysRevB.17.2212>.
- (6) Kürkcü, C.; Merdan, Z.; Öztürk, H. Theoretical Calculations of High-Pressure Phases of NiF_2 : An Ab Initio Constant-Pressure Study. *Russ. J. Phys. Chem.* **2016**, *90* (13), 2550–2555. <https://doi.org/10.1134/S0036024416130057>.
- (7) Tressaud, A.; Soubeyroux, J. L.; Touhara, H.; Demazeau, G.; Langlais, F. On a New Structural Type of Fluorine Compounds: Crystal and Magnetic Structures of a High Pressure Form of PdF_2 . *Materials Research Bulletin* **1981**, *16* (2), 207–214. [https://doi.org/10.1016/0025-5408\(81\)90083-0](https://doi.org/10.1016/0025-5408(81)90083-0).
- (8) Kurzydłowski, D. The Jahn-Teller Distortion at High Pressure: The Case of Copper Difluoride. *Crystals* **2018**, *8* (3), 140. <https://doi.org/10.3390/cryst8030140>.
- (9) Grzelak, A.; Gawraczyński, J.; Jaroń, T.; Kurzydłowski, D.; Budzianowski, A.; Mazej, Z.; Leszczyński, P. J.; Prakapenka, V. B.; Derzsi, M.; Struzhkin, V. V.; Grochala, W. High-Pressure Behavior of Silver Fluorides up to 40 GPa. *Inorg. Chem.* **2017**, *56* (23), 14651–14661. <https://doi.org/10.1021/acs.inorgchem.7b02528>.
- (10) Perakis, A.; Lampakis, D.; Boulmetis, Y. C.; Raptis, C. High-Pressure Raman Study of the Ferroelastic Rutile-to- CaCl_2 Phase Transition in ZnF_2 . *Phys. Rev. B* **2005**, *72* (14), 144108. <https://doi.org/10.1103/PhysRevB.72.144108>.
- (11) Kurzydłowski, D.; Oleksiak, A.; Pillai, S. B.; Jha, P. K. High-Pressure Phase Transitions of Zinc Difluoride up to 55 GPa. *Inorg. Chem.* **2020**, *59* (4), 2584–2593. <https://doi.org/10.1021/acs.inorgchem.9b03553>.
- (12) Kusaba, K.; Kikegawa, T. In Situ X-Ray Observation of Phase Transitions in under High Pressure and High Temperature. *Solid State Communications* **2008**, *145* (5–6), 279–282. <https://doi.org/10.1016/j.ssc.2007.11.009>.
- (13) Liu, G.; Wang, H.; Ma, Y.; Ma, Y. Phase Transition of Cadmium Fluoride under High Pressure. *Solid State Communications* **2011**, *151* (24), 1899–1902. <https://doi.org/10.1016/j.ssc.2011.09.027>.
- (14) Wu, X.; Wu, Z. Theoretical Calculations of the High-Pressure Phases of ZnF_2 and CdF_2 . *Eur. Phys. J. B* **2006**, *50* (4), 521–526. <https://doi.org/10.1140/epjb/e2006-00179-8>.
- (15) Schyck, S.; Evlyukhin, E.; Kim, E.; Pravica, M. High Pressure Behavior of Mercury Difluoride (HgF_2). *Chemical Physics Letters* **2019**, *724*, 35–41. <https://doi.org/10.1016/j.cplett.2019.03.045>.
- (16) Gawraczyński, J.; Kurzydłowski, D.; Ewings, R. A.; Bandaru, S.; Gadomski, W.; Mazej, Z.; Ruani, G.; Bergenti, I.; Jaroń, T.; Ozarowski, A.; Hill, S.; Leszczyński, P. J.; Tokár, K.; Derzsi, M.; Barone, P.; Wohlfeld, K.; Lorenzana, J.; Grochala, W. Silver Route to Cuprate Analogs. *Proc Natl Acad Sci USA* **2019**, *116* (5), 1495–1500. <https://doi.org/10.1073/pnas.1812857116>.